THE JOURNAL OF PHYSICAL CHEMISTRY C

ARTICLE

pubs.acs.org/JPCC

# The Kinetics and Mechanism of Long-Range Pore Ordering in Anodic Films on Aluminum

Kirill S. Napolskii,*[,†,‡] Ilya V. Roslyakov,[†] Andrey A. Eliseev,[†] Dmytro V. Byelov,[§] Andrei V. Petukhov,[§] Natalia A. Grigoryeva,[∥] Wim G. Bouwman,[⊥] Alexey V. Lukashin,[†] Andrey P. Chumakov,[#] and Sergey V. Grigoriev[#]

[†]Department of Materials Science, Moscow State University, Leninskie Hills, Moscow, 119991, Russia

[‡]Department of Chemistry, Moscow State University, Leninskie Hills, Moscow, 119991, Russia

[§]Van't Hoff Laboratory for Physical and Colloid Chemistry, Debye Institute for Nanomaterials Science, University of Utrecht, Padualaan 8, Utrecht, 3584 CH, The Netherlands

[∥]St. Petersburg State University, St. Petersburg, 198504, Russia

[⊥]Delft University of Technology, Mekelweg 15, Delft, 2629 JB, The Netherlands

[#]Petersburg Nuclear Physics Institute, Gatchina, St. Petersburg, 188300, Russia

Supporting Information

**ABSTRACT:** Anodic aluminum oxide has unique and highly attractive properties, including self-ordering of porous structure during anodization. Although anodization regimes leading to formation of highly ordered porous structures had been found experimentally, many aspects of the self-organization mechanism remain unsolved. Here, the detailed in situ small-angle X-ray diffraction study of the self-ordering in porous alumina films is reported. Structure evolution kinetics was deduced by a quantitative analysis of diffraction patterns combined with electron microscopy. The rate of pore ordering is shown to have maximal value at the initial anodization stage and rapidly decreases inversely proportional to $t^{0.2}$. Self-organization is shown to occur via growth of domains possessing preferential in-plane orientation and "death" of other domains, similar to Ostwald ripening governed by difference in pore growth rates for domains of different orientations. The process is accompanied by pore death and splitting making a significant impact on anodic oxides utilization in any mass-transport issues. This finding opens a novel approach for growth of highly ordered porous anodic oxide films.

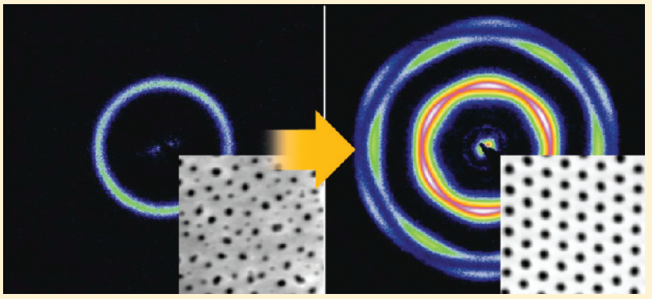

## INTRODUCTION

Anodic aluminum oxide (AAO) is a typical self-ordered mesoporous material. Since the pioneering work[1] of Masuda and Fukuda in 1995, which showed the opportunity of the formation of large scale ordered structures, AAO has been intensively used as a platform for creating various nanostructured functional devices.[2−5] Detailed understanding of the self-organization process is crucial for the further improvement of their functional properties. For example, long-range ordering is prerequisite for utilization of AAO as high-permeability porous membranes and many template issues.

Despite the significant progress achieved in recent years,[6−13] many aspects of the self-organization mechanism remain unsolved. In order to explain a formation of the ordered structure in anodic oxides the models relying on electric-field-dependent interface evolution,[14] mechanical stress-guided repulsion,[7] and viscous flows of oxide species[8] were reported. However none of them concerns evolution of the porous structure during self-organization due to their 2D nature, and cannot explain splitting of AAO channels. In 2008 a next step in understanding of porous structure formation was made by Su and Zhou, who proposed an equifield strength model based on field assisted dissociation of water molecules at AAO pore bottoms.[9,10] To describe pore ordering, the model also relies upon a stress-enhanced arrangement mechanism, which still cannot justify formation and evolution of domain structure.

Recently, we have demonstrated that the small angle neutron and X-ray diffraction techniques are excellent tools for the structural characterization of the self-ordered porous oxide films.[15,16] It was shown that the anodization of technical grade aluminum leads to the formation of disordered porous structure with narrow distributions of pore diameter and interpore distance. On the contrary, the use of high-purity aluminum with a coarse-grained structure leads to self-organization of the lateral

**Received:** August 12, 2011
**Revised:** October 17, 2011
**Published:** October 19, 2011

positions of the pores into a hexagonal structure with well-defined preferential in-plane orientation of the hexagons formed by six neighboring pores extending over macroscopic distances larger than several millimeters. This ordering will be referred to as in-plane orientational order throughout this paper. We have shown that despite the long-ranged in-plane orientational order the interpore positional order is rather short-ranged and does not extend ~10 periods. In the direction of the film growth, the pores have a very long self-correlation length of the order of tens of micrometers. All these facts cannot be explained in the frame of either equifield strength or mechanical stress models.

Therefore we performed a detailed in situ small-angle X-ray diffraction study of the self-ordering behavior in AAO membranes during the two-step anodization[17] of high purity aluminum under mild conditions: in oxalic and sulfuric acids at 40 and 25 V, respectively. These regimes are often used for the preparation of well-ordered porous structures with 105 and 65 nm periodicity.[7,18] The in situ approach provides new insights into the problem in comparison to the reported investigations, where the superstructure was studied ex situ, after the formation of the membranes.[19,20] Owing to the challenge to resolve the width of diffraction maxima at tiny angles, together with the high sample and electrolyte absorption and the need for temporal resolution in (sub)minute scale, a microradian X-ray diffraction setup on a synchrotron source was used. Our results quantitatively characterize the kinetics of the self-organization process during the first and second anodization. The in situ data are collected using microradian X-ray diffraction, which provides authentic and accurate determination of structural parameters during evolution of porous structure. The results, in combination with ex situ Scanning electron microscopy (SEM) measurements, allow us to suggest the mechanism of the evolution of porous structure, which was simulated numerically and gave a close agreement with the observed kinetics of the self-organization process. Self-organization is shown to occur via growth of domains possessing preferential in-plane orientation and "death" of other domains, similar to Ostwald ripening.

## EXPERIMENTAL SECTION

Preliminarily annealed at 550 °C in air and mechanically polished to a mirror finish, high-purity aluminum foils (99.999%, 0.5 mm thick, Goodfellow) were used as the starting material. The aluminum oxidation was performed in a two-electrode cell, which is specially designed for small-angle XRD in situ experiments (see Figure S1, Supporting Information). Pt wire was used as a counter electrode. The anodization was carried out in 0.3 M oxalic ($(COOH)_2$, 98%, Aldrich) and 0.3 M sulfuric ($H_2SO_4$, 95−97%, Fluka) acids at constant voltages of 40 and 25 V, respectively. The electrolyte was pumped through the cell, and its temperature was kept in the range of 0−1 °C. After the first anodization, alumina films were selectively etched away in a 0.6 M $H_3PO_4$ + 0.2 M $CrO_3$ solution at 70 °C. The second anodization was performed under the same conditions.

The diffraction experiments were performed at the beamline BM26B "DUBBLE"[21] of the European Synchrotron Radiation Facility (ESRF) in Grenoble (France) using a microradian X-ray diffraction setup similar to the one described in refs 22 and 23. A 13 keV X-ray beam (wavelength $\lambda$ = 0.95 Å, bandpass $\Delta\lambda/\lambda = 2 \times 10^{-4}$, size 0.5 × 0.5 mm$^2$ at the sample) was used. The beam was focused by a set of beryllium compound refractive lenses[24,25] installed in the experimental hutch just in front of the sample.

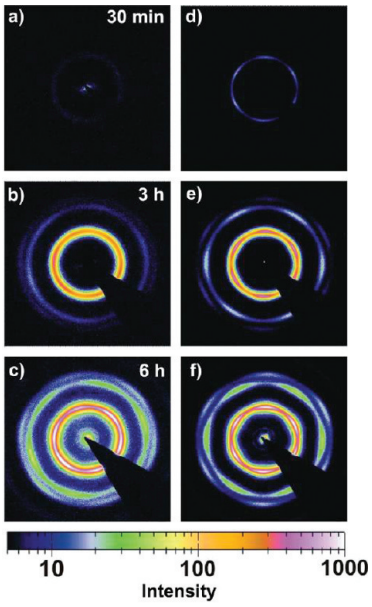


**Figure 1.** Diffraction patterns obtained during the first (left column) and second (right column) anodization of mechanically polished high-purity aluminum in 0.3 M oxalic acid at 40 V. Exposure time is 60 s. Anodization time is 30 min (a, d), 3 h (b, e), and 6 h (c, f).

The lenses focused the beam at the phosphor screen of a two-dimensional CCD detector (Photonic Science, 4008 × 2672 pixels of 22 × 22 $\mu$m). The detector was installed 8 m from the sample position. The electrochemical cell was mounted on a goniometer head to allow for careful orientation around the horizontal and vertical axes orthogonal to the beam. In order to minimize attenuation of the X-ray beam in an electrolyte solution the distance between the back capton window and the aluminum plate was decreased to 5 mm. The transmission through the cell (5 mm of electrolyte and 0.5 mm thick sample) was ca. 6%. Diffraction patterns were collected every 2 min. As a result, two series of diffraction patterns for both anodization conditions were obtained for the first and second anodization, respectively.

SEM images of AAO porous films were recorded with a LEO Supra 50 VP instrument. The height profile of aluminum surface after selective oxide film dissolution was performed using an atomic force microscope, NT-MDT NTEGRA Aura. The AFM was operated in tapping mode using MikroMasch silicon cantilevers (NSC15). All images were taken in air at room temperature. Flatten correction by 2D surface subtraction and further image analysis were performed using the NT-MDT Nova software package.

## RESULTS AND DISCUSSION

Figure 1 shows two series of diffraction patterns obtained during the first and second anodization, respectively (see also movie in the Supporting Information). According to electron backscatter diffraction data, the annealed aluminum foils used as substrates contain single crystal grains of several millimeters in size in the lateral directions. Taking into account the size of the irradiated area (0.5 × 0.5 mm$^2$), we can suppose that diffraction patterns are obtained from the oxide film grown on a single crystal substrate. In this case the influence of grain boundaries on pore ordering in the oxide film[15] is negligible.

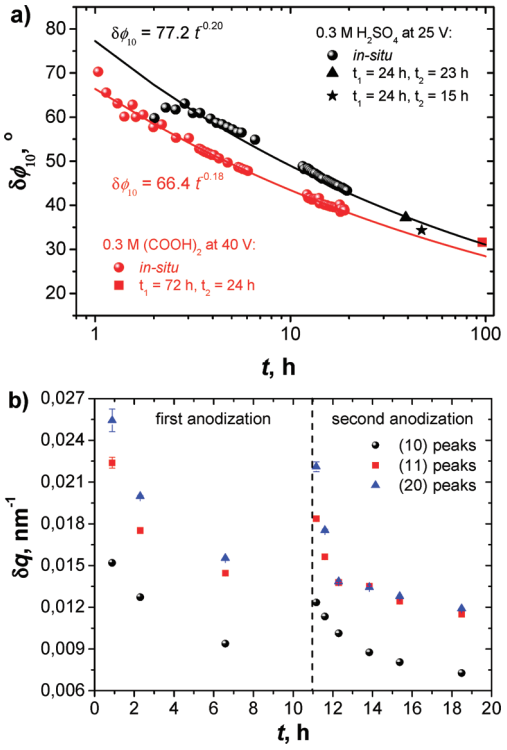


**Figure 2.** Width of diffraction maxima as a function of anodization time. (a) Azimuthal width of the most intense (10) reflections. Results obtained during in situ experiments are depicted as circles, other experimental points correspond to parameters of the samples obtained ex situ. t1 and t2 are the duration of the first and second anodization, respectively. The dashed line is the fit to eq 1. (b) Radial width of diffraction maxima in the case of anodization in 0.3 M sulfuric acid at 25 V.

The diffraction pattern, which is obtained at the initial stage of the first anodization (Figure 1a), exhibits a single intensity ring, while the high order reflections are not visible. Such a pattern corresponds to scattering by a porous film with no long-range correlations. After 3 h of first anodization several intensity rings with ratios of radii of 1:$\sqrt{3}$:2 are clearly observed (Figure 1b), indicating the formation of small regions with hexagonal ordering of the pores. However, separate regions are completely disoriented with respect to each other in the plane of the oxide film. As a result, we observe a ringlike diffraction pattern typical for a powder. Finally, long anodization time leads to the reorientation of pores and the formation of porous film with long-ranged in-plane orientational order and, as a consequence, to spotlike diffraction (see Figure 1c), characteristic for a single domain. The observation of diffraction maxima, rather than rings, indicates a highly ordered superstructure with an orientational correlation length comparable to the beam size.

On the contrary, in the case of the second anodization since the first minutes of oxidation process, we observe only diffraction patterns with modulated intensity along the rings (Figure 1d), testifying that the nucleation of the pores occurs in the small cavities formed at the aluminum surface after the first anodization and the selective dissolution of the oxide film. Up to the forth-order reflections are clearly detected (see panels c and f of Figure 1), suggesting the presence of strong correlations in the channel positions over significant distances. It should be mentioned that even after a long anodization the diffraction peaks are significantly broadened in the azimuthal direction (Figure 1f), which is induced by fluctuations of the in-plane orientational order.

The faint rings near the beamstop in panels c and f of Figure 1 is an artifact caused by slight beam contamination with third-harmonic X-rays (photon energy 39 keV). The apparent $q$ value of this spurious ring is exactly 1/3 of the $q$ value in the most intense (10) reflection. The fake reflections are slightly visible only because of the very weak sample scattering at low $q$. The absence of any significant low-$q$ scattering is an additional indication of the sample quality as it suggests high uniformity of the AAO membrane and relatively low density of defects.

In order to quantitatively characterize the AAO structure at various stages of the anodization process, azimuthal and radial distributions of intensity on the X-ray diffraction patterns were analyzed. The protocol for the treatment of diffraction data is described in detail in our recent work.[16]

Figure 2a shows the azimuthal width of the most intense (10) reflections ($\delta\phi_{10}(t)$) as a function of the anodization time. The obtained dependences $\delta\phi_{10}(t)$ for both anodization conditions sufficiently fit by the power function

$$\delta\phi_{10}(t) = at^b \tag{1}$$

where $a$ and $b$ are constants.

Approximation of the experimental data using eq 1 is shown in Figure 2a as lines. Along with the results of the in situ experiment, several points obtained ex situ are also presented and closely follow the trend described by eq 1. It is clearly seen that the parameter $b$ for both anodization conditions is close to −0.2. This points out the similarities in self-organization mechanism for the two mild anodization conditions leading to the formation of the ordered structures. At the same time, the mosaicity of the structure of porous films obtained at the initial stages of oxidation is lower in the case of oxalic acid (the smaller value of $a$). Only at $t \sim 100$ h does the mosaicity of the two samples converge.

It is worth noting, that the observed width of diffraction maxima is, in fact, averaged over the whole film thickness. We approximate it here by

$$\delta\phi_{10}(t) = \frac{1}{t}\int_0^t \phi(\tau)\,d\tau \tag{2}$$

where $\phi(\tau)$ is mosaicity of the thin porous oxide layer formed at a given moment $\tau$ and $t$ is the duration of anodization.

From eqs 1 and 2, we can conclude that the mosaicity of the porous oxide layer formed at metal/oxide interface is described with

$$\phi(t) = a(b+1)t^b \sim t^{-0.2} \tag{3}$$

Thus, the rate of self-organization of the porous structure of AAO is maximal at the initial anodization stage and rapidly decreases inversely proportional to $t^{0.2}$.

Fit of the structure factor ($S(q) = I(q)/F(q)$, where $F(q)$ is form factor of pores) with a sum of Lorentzians (for more details see our recent work[16]) yields time dependence of the radial width of the diffraction maxima. Broadening of the Bragg peaks in the radial direction ($\delta q_{ij}$) decreases with the increase of the anodization time (see Figure 2b), which points to the growth of the average domain size. Moreover, the rate of ordering (the reduction of $\delta q_{ij}$) reduces with time. We note that the quantitative determination of the time dependences of the domain size (usually defined as inverse value of the broadening of the Bragg peaks in the radial direction) is highly obstructed due to the

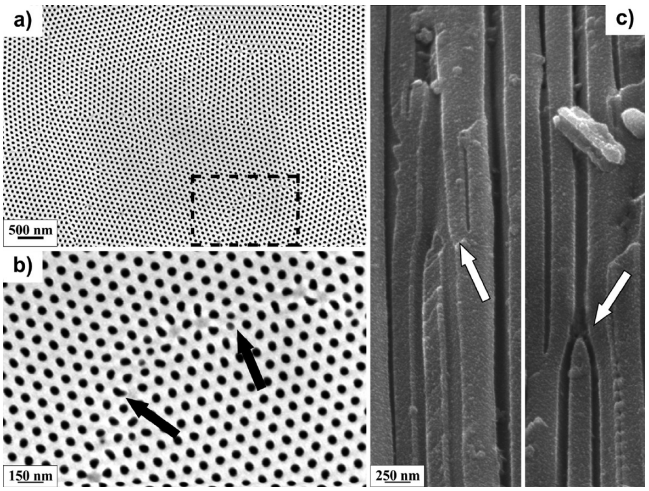


**Figure 3.** SEM images of anodic alumina films. (a) Bottom of an AAO membrane (40 V, 0.3 M $(COOH)_2$) after removal of the barrier layer by chemical etching. Enlarged image of the boundary between domains is shown in panel b. (c) Cross section of porous structure of anodic alumina film (140 V, 0.3 M $(COOH)_2$). Places of pore bifurcations are shown by arrows.

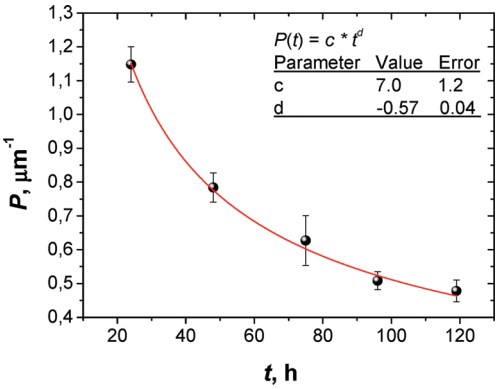


**Figure 4.** Specific perimeter of the boundaries as a function of anodization time calculated from SEM data (40 V, 0.3 M $(COOH)_2$). The error bars represent the spread of the values obtained from different images. The line is a fit of experimental data by the power function.

extremely high influence of the sample orientation on the radial width of the diffraction maxima and the high contribution of microstrain to the broadening of the Bragg peaks even for the lowest-order reflections.[16,26]

It is worth noting, that at the beginning of the second anodization the radial width of the diffraction maxima is somewhat larger in comparison with the one at the end of the first anodization (see Figure 2b). This means that the lattice of pores forming at the initial stage of the second anodization does not completely replicate the lattice of cavities left after the first anodization on the aluminum surface.

The obtained experimental results allow us to suggest the mechanism of pore ordering in anodic films on aluminum. Most probably, self-organization occurs via growth of domains possessing preferential in-plane orientation and "death" of other domains, similar to Ostwald ripening. In the infinite limit, the porous structure tends to an ideal 2D hexagonal structure. Obviously, that transformation of porous structure requires movement of the pore centers in the plane of the oxide film. According to our observations, the domains grow by a death-and-rebirth mechanism (see Figure 3). Growth of a pore, possessing the wrong position, stops, and a bifurcation of a neighboring pore into two channels occurs (Figure 3b). These bifurcation events often happen at the domain boundaries, where the surrounding of the pores is far from the hexagonal one (Figure 3a) and movement of the pores centers in plane of the oxide film is not fully suppressed. Similar structure transformation was discussed earlier,[11] where authors erroneously conclude about pores merging along the domain boundaries.

It is worth noting that the proposed mechanism is in close agreement with observed kinetics of the AAO structure evolution. Probability of the structure transformation at the moment $t$ is proportional to the total perimeter of the domains, which decreases during their growth. The time dependence of the specific perimeter of the domains measured from the SEM images of bottom side of the membranes (see Figure S2, Supporting Information) is shown in Figure 4. The experimental data sufficiently fit to the power function $P(t) = ct^d$, where $d$ is equal to $-0.57 \pm 0.04$. Consequently, as the perimeter of the boundaries is inversely proportion to the average domain size $L$, the latter grows as $\sim t^{0.57}$. It should be noted that the obtained value is in close agreement with work of Li and co-authors,[11] where the average domain area was a linear function of the time.

In order to estimate how the domain size influences the overall spread of azimuthal orientations, let us assume that in average at the domain boundary the orientation of the hexagonal lattice of pores can change by some small value $\Delta$. It can vary clockwise or counterclockwise so that in average, after making $N$ steps, the domain orientations can change by about $(N)^{1/2}\Delta$. In the presented diffraction experiment the overall spread of azimuthal orientations will then be on the order of $\phi(t) \sim (R_{beam}/L)^{1/2}\Delta$, where $R_{beam}$ is the X-ray beam radius. Taking account of $L \sim t^{0.57}$ rough estimation leads to $\phi(t) \sim t^{-0.28}$, which is very close to the observed value from the diffraction experiment (see eq 3).

However the kinetics and mechanism of "domain wall" movement provide no knowledge on the nature of self-organization in AAO films. Most probably, the reason for growth of domains possessing optimal in-plane orientation and gradual vanishing of other domains could be ascribed to a variation of pore growth rate for domains of different orientations. Obviously, for the two pores situated on the opposite sides of the domain border, the probability of bifurcation is higher for that one which is deeper. The deeper channel at the bottom is surrounded by the metal from its side that makes growth of oxide in lateral directions possible (Figure 5e). This pore has an opportunity to split enlarging the area of domain with optimal in-plane orientation, while the neighboring pore standing in the "wrong" position will stop growing. Consequently, the domains consisting of the deeper channels should determine the optimal in-plane orientation of lattice of pores. In order to visualize the difference in growth rate of the domains with different in-plane orientation, an AFM imaging technique was applied (see Figure 5). The maximum height and surface roughness of aluminum surface after oxide film dissolution is found to be about 80 and 6 nm over a $8 \times 8$ $\mu m^2$, respectively. The bottom part of the AFM scan with height of 10 nm is shown in Figure 5b. It is clearly seen that some domains vanished in the height-filtered image. In order to find out the average in-plane orientation of a lattice of pores, fast Fourier transformation (FFT) of AFM images was performed. Wide maxima in the FFT image from initial scan are clearly

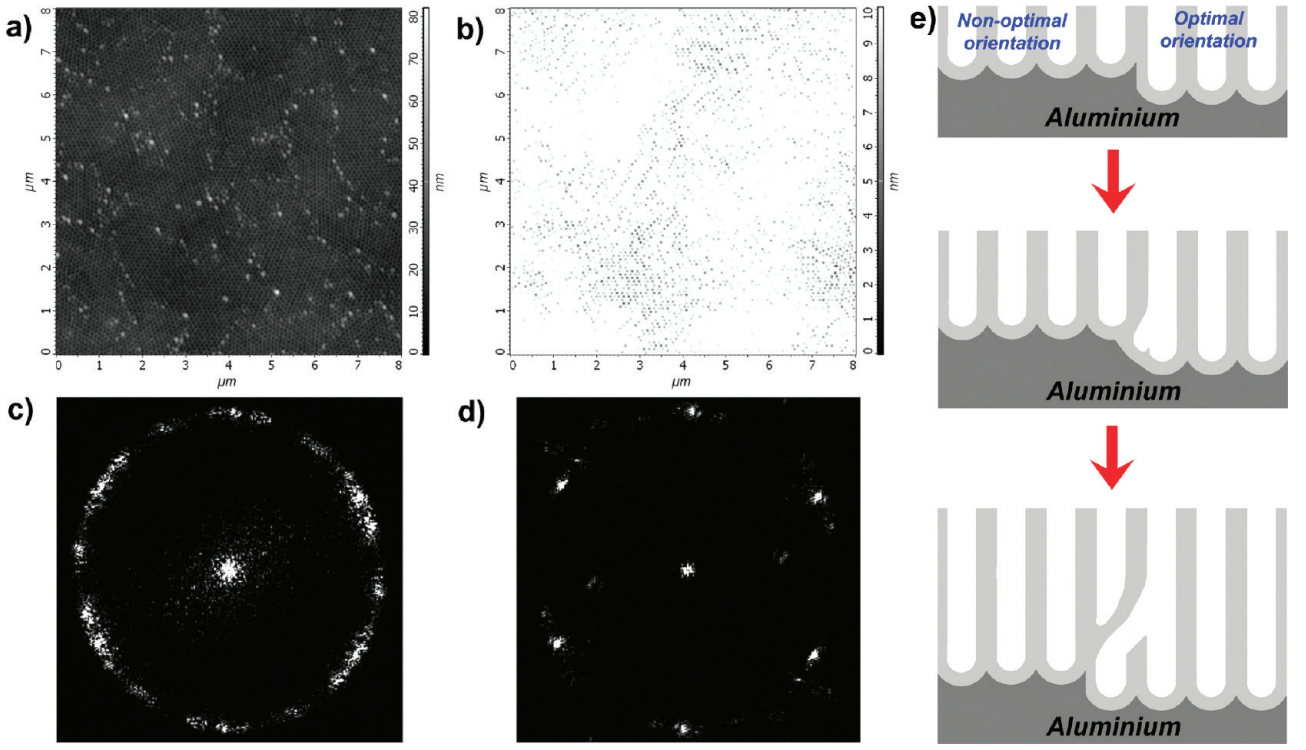


**Figure 5.** AFM image of aluminum surface after selective dissolution of porous oxide film (a) and height-filtered image consisting of only the bottom part of the scan (b). Panels c and d display the intensity of the Fourier transforms of the initial and the height-filtered images, respectively. Panel e illustrates schematic representation of the mechanism of domain growth.

observed, but they become sharper in the case of a FFT image from a height-filtered AFM scan (see panels c and d of Figure 5). Moreover the positions of the main maxima in Figure 5c are equal to positions of sharp maxima in Figure 5d testifying that the average in-plane orientation of a lattice of pores coincides with the orientation of lattice of pores in the deepest domains. One should note the in-plane orientation of deepest domains was found the same at various positions on the aluminum surface after anodization.

In order to check this assumption, numerical simulation of the pore ordering process was carried out (see Figures S3 and S4 in the Supporting Information). The model was based on domain wall movement guided by a difference of pore growth rates for domains of different in-plane orientations. The effect of orientational misalignment on AAO growth rate was defined using the only parameter, $\sigma$, a standard deviation from optimal orientation in Gaussian distribution of growth rates. Time dependence of perimeter and structure mosaicity, obtained within the framework of the proposed model, was found to coincide with experimental results, being fitted well with power function. The "best fit" parameter of $\sigma = 30°$ resulted in $d = -0.54 \pm 0.04$ and $b = -0.28 \pm 0.02$ for $P(t)$ and $\phi(t)$ dependence, which are rather close to experimentally observed values. This states an appropriate choice of the model for structure evolution in anodic alumina films.

It should be noted that the obtained coefficients fit both anodization regimes reported (i.e., 25 V in sulfuric and 40 V in oxalic acid), while the applied voltages, pH of electrolytes, and growth rates of AAO differ substantially. On the other hand both chosen regimes stay in self-organization windows, which were found empirically for anodization in sulfuric and oxalic acids and were shown to result in the best ordering of the porous structures. Therefore one can conclude the mechanism of self-organization of the porous structure is similar in those two cases and have no major dependence on electrolyte chemical nature or anodization voltage. The kinetics of in-plane ordering at optimal mild anodization conditions is also very similar.

Summing up the phenomenon of optimal in-plane orientation existence with the genesis of orientational correlations extending to macroscopic distances for AAO formed on pure recrystallized aluminum, one can deduce close relation of long-range ordering with the nature of metal substrate. Most likely crystallographic orientation of aluminum plays a crucial role; however this fact requires further examination. A detailed investigation of anodic oxidation of single crystalline high-purity aluminum is currently being carried out in our laboratory.

One should note the demonstrated mechanism of pore organization involves formation of large number of dead-ended channels, which cannot be opened by any etching procedures, applied usually for barrier layer removal. Obviously this will negatively affect the transport efficiency of any species (e.g., ions, gas molecules, etc.) through AAO membranes. Taking account of extensive use of anodic porous films as membranes and templates for creation of various one-dimensional nanostructures, the pore ordering will significantly influence loading value or permeability. Moreover, this kind of blocked pore makes porous membranes with disordered structure (e.g., commercially available membranes by Whatman) unsuitable for template or membrane purposes where high loading or permeability is required. The increase of permeability can be simply achieved by increasing total pore ordering by two-step or nanoimprint-guided anodization. The current result extends anodic oxidation

of any metals or alloys and all the mass-transport issues, including gas and liquid permeation, ion exchange, electroless and electrochemical deposition, etc.

## CONCLUSIONS

A detailed in situ small-angle X-ray diffraction study of the self-ordering in porous alumina films formed by single- and two-step anodization of high-purity aluminum was performed. The rate of self-organization of the porous structure of anodic alumina is shown to have maximal value at the initial anodization stage and rapidly decreases inversely proportional to $t^{0.2}$. The picture of pore ordering during anodization could be described in two major processes: (1) domain structure formation and (2) Ostwald ripening of domains guided by a variation of pore growth rate for domains of different in-plane orientations.

In summary, the present work makes a contribution to the research field of anodic metal oxides in both fundamental and practical aspects. First, the observed kinetics and suggested mechanism of pore ordering allow us to understand anodization process in more detail. Second, we can predict that anodic films with highly ordered porous structure are more preferable for their use in mass transport related applications, e.g., templates and membranes, owing to a much smaller amount of the dead-ended pores. Third, the presented data shed a light on the experimental conditions (e.g., anodization duration) required for the preparation of anodic alumina films with desired pore ordering. Finally, the present study is a good demonstration of the possibilities of modern SAXS instruments for the investigation of mesoscopic materials.

## ASSOCIATED CONTENT

**Supporting Information.** Figure S1 shows the conceptual scheme of in situ diffraction experiment, Figure S2 shows SEM images of bottom side of AAO films at different oxidation times, Figures S3 and S4 show numerical simulations of pore ordering process, and the movie illustrates evolution of diffraction patterns during anodization. This information is available free of charge via the Internet at http://pubs.acs.org.

## AUTHOR INFORMATION

**Corresponding Author**
*E-mail: knapolsky@gmail.com.

## ACKNOWLEDGMENT

This work is partially supported by RF President Grants MK-6626.2010.3 and MK-4737.2010.3, by the Russian Foundation for Basic Research (Grant Nos. 09-03-01123, 09-03-12246, and 10-02-00634) and by Russian Ministry of Education and Science (Grant Nos. 16.513.11.3011 and 16.512.11.2164). K.S.N. acknowledges "OPTEC" LLC for financial support. We thank the personnel of the DUBBLE beamline and, in particular, Dirk Detollenaere and Kristina Kvashnina for their excellent support. The authors are grateful to Anatoly Snigirev (ESRF) for his help with X-ray optics, and to Galina A. Tsirlina (Moscow State University) for numerous fruitful discussions and to Oleg Brylev (Moscow State University) for his help with manuscript preparation. We thank Artem A. Eliseev for performing numerical simulation, and Vasiliy A. Lebedev for AFM measurements and Alexey S. Mankevich for EBSD analysis. The "Nederlandse organisatie voor Wetenschappelijk Onderzoek (NWO)" is thanked for granting us the beam time.

## REFERENCES

(1) Masuda, H.; Fukuda, K. *Science* **1995**, *268*, 1466–1468.
(2) Qin, L. D.; Park, S.; Huang, L.; Mirkin, C. A. *Science* **2005**, *309*, 113–115.
(3) McGary, P. D.; Tan, L. W.; Zou, J.; Stadler, B. J. H.; Downey, P. R.; Flatau, A. B. *J. Appl. Phys.* **2006**, *99*, 08B310.
(4) Masuda, H.; Yamada, M.; Matsumoto, F.; Yokoyama, S.; Mashiko, S.; Nakao, M.; Nishio, K. *Adv. Mater.* **2006**, *18*, 213–216.
(5) Banerjee, P.; Perez, I.; Henn-Lecordier, L.; Lee, S. B.; Rubloff, G. W. *Nat. Nanotechnol.* **2009**, *4*, 292–296.
(6) Lee, W.; Ji, R.; Gosele, U.; Nielsch, K. *Nat. Mater.* **2006**, *5*, 741–747.
(7) Jessensky, O.; Muller, F.; Gösele, U. *Appl. Phys. Lett.* **1998**, *72*, 1173–1175.
(8) Houser, J. E.; Hebert, K. R. *Nat. Mater.* **2009**, *8*, 415–420.
(9) Su, Z.; Zhou, W. *Adv. Mater.* **2008**, *20*, 3663–3667.
(10) Su, Z. X.; Hahner, G.; Zhou, W. Z. *J. Mater. Chem.* **2008**, *18*, 5787–5795.
(11) Li, F.; Zhang, L.; Metzger, R. M. *Chem. Mater.* **1998**, *10*, 2470–2480.
(12) Hebert, K. R.; Houser, J. E. *J. Electrochem. Soc.* **2009**, *156*, C275–C281.
(13) Schwirn, K.; Lee, W.; Hillebrand, R.; Steinhart, M.; Nielsch, K.; Gösele, U. *ACS Nano* **2008**, *2*, 302–310.
(14) O'Sullivan, J. P.; Wood, G. C. *Proc. R. Soc. London, Ser. A* **1970**, *317*, 511–543.
(15) Grigoriev, S. V.; Grigorieva, N. A.; Syromyatnikov, A. V.; Napolskii, K. S.; Eliseev, A. A.; Lukashin, A. V.; Tret'yakov, Y. D.; Eckerlebe, H. *JETP Lett.* **2007**, *85*, 449–453.
(16) Napolskii, K. S.; Roslyakov, I. V.; Eliseev, A. A.; Petukhov, A. V.; Byelov, D. V.; Grigoryeva, N. A.; Bouwman, W. G.; Lukashin, A. V.; Kvashnina, K. O.; Chumakov, A. P.; Grigoriev, S. V. *J. Appl. Crystallogr.* **2010**, *43*, 531–538.
(17) Masuda, H.; Satoh, M. *Jpn. J. Appl. Phys.* **1996**, *35*, L126–L129.
(18) Nielsch, K.; Choi, J.; Schwirn, K.; Wehrspohn, R. B.; Gösele, U. *Nano Lett.* **2002**, *2*, 677–680.
(19) Leitao, D. C.; Apolinario, A.; Sousa, C. T.; Ventura, J.; Sousa, J. B.; Vazquez, M.; Araujo, J. P. *J. Phys. Chem. C* **2011**, *115*, 8567–8572.
(20) Hillebrand, R.; Muller, F.; Schwirn, K.; Lee, W.; Steinhart, M. *ACS Nano* **2008**, *2*, 913–920.
(21) Bras, W.; Dolbnya, I. P.; Detollenaere, D.; van Tol, R.; Malfois, M.; Greaves, G. N.; Ryan, A. J.; Heeley, E. *J. Appl. Crystallogr.* **2003**, *36*, 791–794.
(22) Petukhov, A. V.; Thijssen, J. H. J.; 't Hart, D. C.; Imhof, A.; van Blaaderen, A.; Dolbnya, I. P.; Snigirev, A.; Moussaid, A.; Snigireva, I. *J. Appl. Crystallogr.* **2006**, *39*, 137.
(23) Thijssen, J. H. J.; Petukhov, A. V.; Hart, D. C.; 't; Imhof, A.; van der Werf, K.; Schropp, R. E. I.; van Blaaderen, A. *Adv. Mater.* **2006**, *18*, 1662–1666.
(24) Snigirev, A.; Kohn, V.; Snigireva, I.; Lengeler, B. *Nature* **1996**, *384*, 49–51.
(25) Bosak, A.; Snigireva, I.; Napolskii, K. S.; Snigirev, A. *Adv. Mater.* **2010**, *22*, 3256–3259.
(26) Benfield, R. E.; Grandjean, D.; Dore, J. C.; Esfahanian, H.; Wu, Z.; Kroll, M.; Geerkens, M.; Schmid, G. *Faraday Discuss* **2004**, *125*, 327–342.